Inorg. Chem. **2009**, *48*, 861−871

Theoretical Studies of N_2 Reduction to Ammonia in $Fe(dmpe)_2N_2$

Robert B. Yelle,[†] Justin L. Crossland,[‡] Nathaniel K. Szymczak,[‡] and David R. Tyler*[,‡]

Computational Science Institute, University of Oregon, 5294 University of Oregon, 1600 Millrace Drive Suite 105, Eugene, Oregon 97403, and Department of Chemistry, University of Oregon, Eugene, Oregon 97403

Received May 21, 2008

Electronic structure calculations using density functional theory were performed on potential intermediates in the reaction of $Fe(dmpe)_2N_2$ (dmpe = 1,2-bis(dimethylphosphino)ethane) with protons. Three mechanisms were investigated and compared, and the possibility of a two-electron reduction by a sacrificial $Fe(dmpe)_2N_2$ complex was considered in each mechanism. A Chatt-like mechanism, involving the stepwise addition of protons to the terminal nitrogen, was found to be the least favorable. A second pathway involving dimerization of the $Fe(dmpe)_2N_2$ complex, followed by the stepwise addition of protons leading to hydrazine, was found to be energetically favorable; however many of the dimeric intermediates prefer to dissociate into monomers. A third mechanism proceeding through diazene and hydrazine intermediates, formed by alternating protonation of each nitrogen atom, was found to be the most energetically favorable.

Introduction

The conversion of N_2 to ammonia under mild conditions is a coveted goal for chemists,[1] and transition metal complexes have been actively investigated as catalysts for carrying out the transformation. Various group 4 and group 6 transition metal complexes have shown promise in this regard, with $[HIPTN_3N]Mo(N_2)$ ($HIPTN_3N$ = [{3,5-(2,4,6-^{i}Pr$_3$C$_6$H$_2$)$_2$C$_6$H$_3$NCH$_2$CH$_2$}$_3$N]$^{3-}$) being the only well-defined catalytic system to date.[2] Some intriguing reactivity has also been reported using iron complexes.[3,4] Leigh and Jimenez-Tenorio first demonstrated that $Fe(dmpe)_2N_2$ (dmpe = 1,2-bis(dimethylphosphino)ethane) can be protonated to yield ammonia.[5] Further work in our laboratory on a similar system using $Fe(DMeOPrPE)_2(N_2)$ (DMeOPrPE = 1,2-bis(bis-(methoxypropyl)phosphino)ethane) demonstrated that, upon protonation, N_2 could be reduced to ammonia and hydrazine at atmospheric temperature and pressure (eq 1).[6] Noteworthy is that access to the $Fe^0P_4(N_2)$ precursor was gained through an $Fe^{II}P_4(H_2)H^+$ intermediate, formed by the reaction of $Fe^{II}P_4Cl_2$ with H_2. Thus, H_2 is the source of electrons for the reduction of N_2 to ammonia.

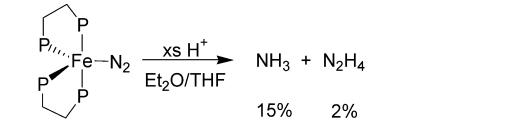

(1)

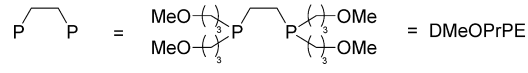

To achieve a catalytic N_2 fixation scheme based on eq 1, a better understanding of the mechanism of the N_2 reduction pathway is needed.[7,8] Understanding the mechanism of N_2 reduction in these complexes may also give insights into the mechanism of nitrogenase.[9] Increasing biochemical evidence has determined that iron is likely the site of N_2 binding and reduction in this enzyme.[10] Other recent work has shown

* To whom correspondence should be addressed. E-mail: dtyler@uoregon.edu.
† Computational Science Institute.
‡ Department of Chemistry.

(1) Postgate, J. *Nitrogen Fixation*, 3rd ed.; Cambridge University Press: Cambridge, U.K., 1998.
(2) Yandulov, D. V.; Schrock, R. R. *Science* **2003**, *301*, 76–78.
(3) Betley, T.; Peters, J. C. *J. Am. Chem. Soc.* **2004**, *126*, 6252–6254.
(4) Smith, J. M.; Lachicotte, R. J.; Pittard, K. A.; Cundari, T. R.; Lukat-Rodgers, G.; Rodgers, K. R.; Holland, P. L. *J. Am. Chem. Soc.* **2001**, *123*, 9222–9223.
(5) Leigh, G. J.; Jimenez-Tenorio, M. *J. Am. Chem. Soc.* **1991**, *113*, 5862–5863.
(6) Gilbertson, J. D.; Szymczak, N. K.; Tyler, D. R. *J. Am. Chem. Soc.* **2005**, *127*, 10184–10185.
(7) Hall, D. A.; Leigh, G. J. *Dalton Trans.* **1996**, 3539–3541.
(8) Hirano, M.; Akita, M.; Morikita, T.; Kubo, H.; Fukuoka, A.; Komiya, S. *Dalton Trans.* **1997**, 3453–3458.
(9) Igarashi, R. Y.; Seefeldt, L. C. *Crit. Rev. Biochem. Mol. Biol.* **2003**, *38*, 351–384.
(10) Dos Santos, P. C.; Igarashi, R. Y.; Lee, H.; Hoffman, B. M.; Seefeldt, L. C.; Dean, D. R. *Acc. Chem. Res.* **2005**, *38*, 208–214.

10.1021/ic800930t CCC: $40.75
Published on Web 01/07/2009

that hydrazine and diazene are likely intermediates along the N_2 reduction pathway.[11] This evidence points to a different mechanism than the Chatt mechanism (three stepwise additions of a proton and an electron to the terminal N atom)[12] and suggests instead a mechanism in which protonation alternates between the proximal and distal nitrogen atoms of a bound N_2 ligand.[13]

Current hypotheses about the intermediates involved in the mechanism of N_2 reduction for $FeP_4(N_2)$ systems are speculative, and to our knowledge, a detailed theoretical study of the mechanism has not been reported. In order to perform the calculations at a high level of theory, the dmpe ligand was used instead of the DMeOPrPE ligand. We find this simplification to be acceptable because the $Fe(dmpe)_2N_2$ complex has also been shown to produce ammonia in the presence of acid.[5]

Six electrons are required to fully reduce N_2 to two NH_3 molecules. Previous experiments suggest that the protonation of $Fe^0(dmpe)_2N_2$ results in an Fe^{II} product,[6] suggesting that the complex provides only two electrons toward the reduction. Although the mechanism may involve two separate one-electron reductions, in this study, mechanisms involving a two-electron reduction from a sacrificial $Fe(dmpe)_2N_2$ complex were considered. Using density functional theory (DFT), we investigated three possible pathways of N_2 reduction: an asymmetric monomer mechanism (Chatt-like) that involves successive protonation at the terminal nitrogen, a symmetric monomer mechanism that proceeds through diazene and hydrazine intermediates, and a dimer mechanism in which reduction takes place through a bridged N_2 species.

Computational Methods

All calculations were performed using NWChem, versions 4.7 and 5.0.[14−16] Transition states were not examined in this study. Rather, as a first approximation, calculations were performed only on hypothetical intermediates of each mechanism, shown in Schemes 1−4. The building and modeling of $Fe(dmpe)_2N_2$ and all related intermediates was performed using the program Ecce version 3.2.4.[17,18] Calculations were performed on singlet states of each intermediate, although for some monomer intermediates, the triplet or quintet states were considered. Calculations involving open-shell (triplet or quintet) systems were performed using the unrestricted (spin-polarized) framework. In some cases, the triplet state is much higher in energy than the singlet, but in other cases (**2a**, **6a**, and **6b**), the triplet states were found to be slightly lower. However, in those cases where they are lower, they are sufficiently close to the singlet in energy that they would not affect the mechanisms described here. Thus, the analysis and discussion of these intermediates will focus on the singlet states, except where the higher spin states are clearly more important (such as complexes **15** and **16**, in the Supporting Information). Protonation reactions were modeled using triflic acid (TfOH) as the proton source.[6] No external reductant was used by Gilbertson et al.;[6] therefore, the $Fe(dmpe)_2N_2$ reactant (**1**) was also modeled as the reductant ($Fe^0 \rightarrow Fe^{II}$) for steps involving outer-sphere electron transfer. Upon oxidation, the dinitrogen dissociates from the resulting high-spin $Fe^{II}(dmpe)_2$ (complex **16**, see Supporting Information).

Scheme 1. Comparison of Two Initial Protonation Reactions of $Fe(dmpe)_2N_2$ (**1**)[a]

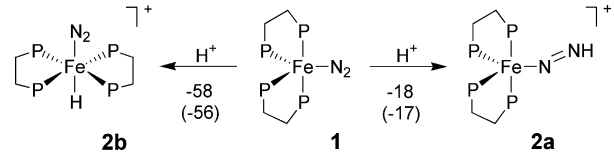

[a] Reaction energies are in kcal/mol, and free energies are given in parentheses.

Scheme 2. Calculated Intermediate Structures for the Asymmetric Protonation of $Fe(dmpe)_2N_2$[a]

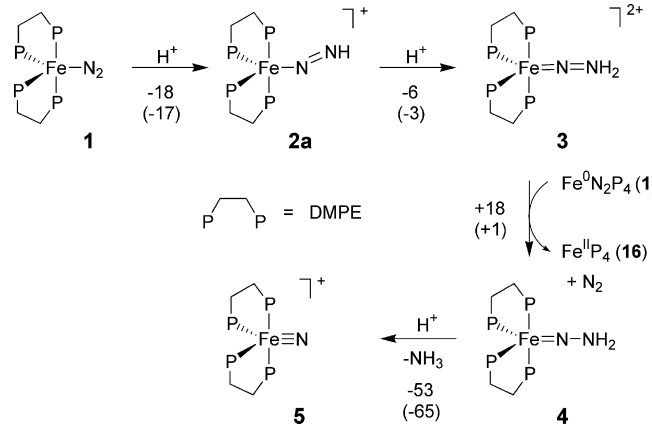

[a] Reaction energies are in kcal/mol, and free energies are given in parentheses.

(11) Barney, B. M.; Lee, H.; Dos Santos, P. C.; Hoffman, B. M.; Dean, D. R.; Seefeldt, L. C. *Dalton Trans.* **2006**, 2277–2284.

(12) Chatt, J.; Dilworth, J. R.; Richards, R. L. *Chem. Rev.* **1978**, *78*, 589–625.

(13) Barney, B. M.; Lukoyanov, D.; Yang, T.; Dean, D. R.; Hoffman, B. M.; Seefeldt, L. C. *PNAS* **2006**, *103*, 17113–17118.

(14) Kendall, R. A.; Apra, E.; Bernholdt, D. E.; Bylaska, E. J.; Dupuis, M.; Fann, G. I.; Harrison, R. J.; Ju, J.; Nichols, J. A.; Nieplocha, J.; Straatsma, T. P.; Windus, T. L.; Wong, A. T. *Comput. Phys. Commun.* **2000**, *128*, 260–283.

(15) A Computational Chemistry Package for Parallel Computers: Aprà, E.; Windus, T. L.; Straatsma, T. P.; Bylaska, E. J.; Jong, W. A. d.; Hirata, S.; Valiev, M.; Hackler, M.; Pollack, L.; Kowalski, K.; Harrison, R.; Dupuis, M.; Smith, D. M. A.; Nieplocha, J.; Tipparaju, V.; Krishnan, M.; Auer, A. A.; Brown, E.; Cisneros, G.; Fann, G. I.; Früchtl, H.; Garza, J.; Hirao, K.; Kendall, R.; Nichols, J. A.; Tsemekhman, K.; Wolinski, K.; Anchell, J.; Bernholdt, D.; Borowski, P.; Clark, T.; Clerc, D.; Dachsel, H.; Deegan, M.; Dyall, K.; Elwood, D.; Glendening, E.; Gutowski, M.; Hess, A.; Jafe, J.; Johnson, B.; Ju, J.; Kobayashi, R.; Kutteh, R.; Lin, Z.; Littlefield, R.; Long, X.; Meng, B.; Nakajima, T.; Niu, S.; Rosing, M.; Sandrone, G.; Stave, M.; Taylor, H.; Thomas, G.; Lenthe, J. v.; Wong, A.; Zhang, Z. *NWChem*, v. 4.7; Pacific Northwest National Laboratory: Richland, WA, 2005.

(16) A Computational Chemistry Package for Parallel Computers: Bylaska, E. J.; Jong, W. A. d.; Kowalski, K.; Straatsma, T. P.; Valiev, M.; Wang, D.; Aprà, E.; Windus, T. L.; Hirata, S.; Hackler, M. T.; Zhao, Y.; Fan, P.-D.; Harrison, R. J.; Dupuis, M.; Smith, D. M. A.; Nieplocha, J.; Tipparaju, V.; Krishnan, M.; Auer, A. A.; Nooijen, M.; Brown, E.; Cisneros, G.; Fann, G. I.; Früchtl, H.; Garza, J.; Hirao, K.; Kendall, R.; Nichols, J. A.; Tsemekhman, K.; Wolinski, K.; Anchell, J.; Bernholdt, D.; Hess, P. A.; Jaffe, J.; Johnson, B.; Ju, J.; Kobayashi, R.; Kutteh, R.; Lin, Z.; Littlefield, R.; Long, X.; Meng, B.; Wong, T. A.; Zhang, Z. *NWChem*, v. 5.0; Pacific Northwest National Laboratory: Richland, WA, 2006.

(17) Schuchardt, K. L.; Didier, B. T.; Black, G. D. Ecce - A Problem-Solving Environment's Evolution Toward Grid Services and a Web Architecture. *Concurrency and Computation: Practice and Experience*; John Wiley & Sons, Ltd.: New York, 2002; Vol. *14*, pp 1221−1239.

(18) Black, G. D.; Didier, B. T.; Elsethagen, T.; Feller, D.; Gracio, D.; Hackler, M.; Havre, S.; Jones, D.; Jurrus, E.; Keller, T.; Lansing, C.; Matsumoto, S.; Palmer, B.; Peterson, M.; Schuchardt, K.; Stephan, E.; Taylor, H.; Thomas, G.; Vorpagel, E.; Windus, T. *Ecce*, v. 3.2; Pacific Northwest National Laboratory: Richland, WA, 2004.

Scheme 3. Proposed Intermediate Structures for the Symmetric Protonation of Fe(dmpe)$_2N_2$[a]

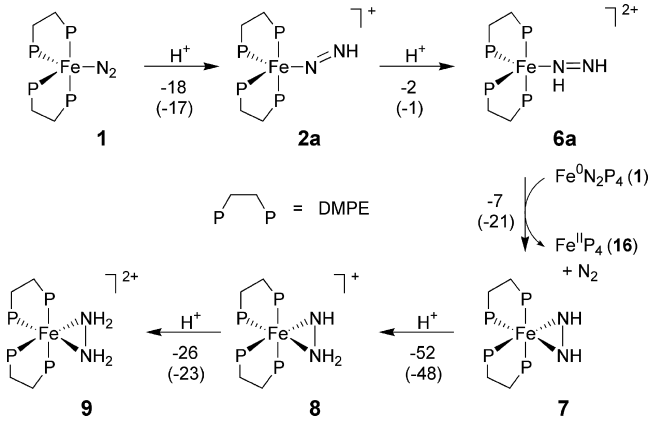

[a] Reaction energies are in kcal/mol, and free energies are given in parentheses.

All calculations employed the B3LYP hybrid functional.[19−22] The geometries of each structure, **1**−**16**, were optimized using the 6-31G* basis set.[23,24] While some of the molecules have C_2 or higher symmetry, symmetry was not enforced in the optimizations because the symmetric structures were not always the lowest-energy structures. For complexes **3** and **4**, the use of a fine grid and tighter convergence criteria were needed to obtain a minimum-energy structure. Single-point energy calculations were performed on each optimized structure. These employed the "Wachters+f" basis set for Fe,[25] which is a (14s11p6d3f)/[8s6p4d1f] contraction, and the 6-311G** basis set[26] for all other atoms. Solvation effects were incorporated into the single-point energy calculations using the COSMO reaction field[27] with a dielectric constant of 7.52 corresponding to tetrahydrofuran (THF).

The evaluation of solvation energies has an important bearing on the reaction energies. Solvation energies are highly dependent on the atomic radii used. The default radii in NWChem are close to the traditional van der Waal radii, which are generally quite small and can lead to an overestimate of the solvation energies. With the exception of iron, where the default NWChem value of 1.8 Å was used, the remaining atomic radii used were those developed by Stefanovich and Truong,[28] which were optimized to give the best fit to experimental hydration energies for a representative group of molecules. Radii corresponding to "hydrogen-bonding" nitrogen atoms were used for all nitrogen atoms because binding to the iron results in polarizing the nitrogen atoms, making them susceptible to hydrogen bonding. In our studies, we found that the Stefanovich−Truong (S-T) radii gave solvation energies for NH_3 that were much closer to experimental hydration energies (−3 kcal/mol) than the default NWChem values (−6 for the S-T radii versus −12 kcal/mol for the default values). In general, the S-T radii are larger than the default values, and they result in a more conservative contribution of solvation energies to the total reaction energies.

Vibrational frequency calculations were performed on the optimized structures **1**−**9** in the singlet states, the triplet state of **15**, and the quintet state of **16**, using the 6-31G* basis set. Complex **16** had one imaginary frequency, but no other structures had any imaginary frequencies. Thermal and entropic corrections were obtained for monomer complexes **1**−**9**, **15**, and **16**. Reaction energies are given with these corrections (free energies) and without these corrections (electronic energies) in Schemes 1−3. Frequency calculations were not performed on the dimeric structures **10**−**14** (Scheme 4) due to the considerable computational expense. Thus, thermal and entropic corrections could not be obtained for these intermediates, so only electronic reaction energies are given there. Most of the differences in reaction energy due to these thermal and entropic corrections presented here were negligible, except for reactions involving the release of N_2 or NH_3 where entropy played a large role. However, due to the electronic energies obtained for the dimer, the neglect of entropy is not likely to change any conclusions drawn from this work (see Discussion). To compare all schemes on equal ground, the discussion of reaction energies will involve mainly the electronic energies, except where stated otherwise.

Mulliken population analysis was used to determine atomic populations from the single-point energy calculations, and N−N, Fe−N, and Fe−P bond orders were computed for each complex. When describing the electronic structure, the z axis is taken to be parallel to the axial Fe−P bonds, with the equatorial Fe−P bonds on the xy plane. For most structures, the x axis is taken to be the Fe−N bond, except for structures with side-on binding (e.g., complexes **7**−**9**), in which case the x axis bisects the N_α−Fe−N_β angle (Figure 1). Most of the molecular orbitals computed for these complexes contain significant contributions from several atomic orbitals, so the descriptions will focus only on the primary components of a given molecular orbital.

Results and Analysis

Calculated data have been summarized in Tables 1−4 so as not to congest the discussion below. Table 1 contains Fe−P and Fe−N bond lengths and Fe−N−N bond angles from the geometry optimization of each intermediate. Calculated Fe−N and N−N vibrational frequencies of the monomer intermediates are given in Table 2. Tables 3 and 4 contain bond orders and atomic charges, respectively, derived from Mulliken population analysis. An energy level correlation diagram for complex **1** is shown in Figure 2. Energy level diagrams for the other monomeric intermediates are provided in the Supporting Information, as well as figures showing bonding molecular orbitals. The energy profiles for all three mechanisms are shown in Figure 3. In the text that follows, N_α and N_β refer to the coordinated (proximal) and noncoordinated (distal) nitrogen atoms in a linearly bonded M−N≡N unit, respectively.

(19) Becke, A. D. *Phys. Rev. A: At., Mol., Opt. Phys.* **1988**, *38*, 3098–3100.
(20) Lee, C.; Yang, W.; Parr, R. G. *Phys. Rev. B: Condens. Matter Mater. Phys.* **1988**, *37*, 785–789.
(21) Becke, A. D. *J. Chem. Phys.* **1993**, *98*, 5648–5652.
(22) Becke, A. D. *J. Chem. Phys.* **1993**, *98*, 1372–1377.
(23) Hariharan, P. C.; Pople, J. A. *Theor. Chim. Acta* **1973**, *28*, 213–222.
(24) Rassolov, V.; Pople, J. A.; Ratner, M.; Windus, T. L. *J. Chem. Phys.* **1998**, *109*, 1223.
(25) Wachters, A. J. H. *J. Chem. Phys.* **1970**, *52*, 1033–1036.
(26) Krishnan, R.; Binkley, J. S.; Seeger, R.; Pople, J. A. *J. Chem. Phys.* **1980**, *72*, 650–654.
(27) Klamt, A.; Schüürmann, G. *J. Chem. Soc., Perkin Trans. 2* **1993**, *5*, 799–805.
(28) Stefanovich, E. V.; Truong, T. N. *Chem. Phys. Lett.* **1995**, *244*, 65–74.
(29) Komiya, S.; Akita, M.; Yoza, A.; Kasuga, N.; Fukuoka, A.; Kai, Y. *J. Chem. Soc., Chem. Commun.* **1993**, 787–788.
(30) Field, L. D.; Li, H. L.; Dalgarno, S. J.; Turner, P. *Chem. Commun.* **2008**, 1680–1682.
(31) Crossland, J. L.; Zakharov, L. N.; Tyler, D. R. *Inorg. Chem.* **2007**, *46*, 10476–78.
(32) Hills, A.; Hughes, D. L.; Jimenez-Tenorio, M.; Leigh, G. J.; Rowley, A. T. *J. Chem. Soc., Dalton Trans.* **1993**, 3041–3049.

Scheme 4. Proposed Intermediate Structures for the Symmetric Protonation of $Fe_2(dmpe)_4N_2$[a]

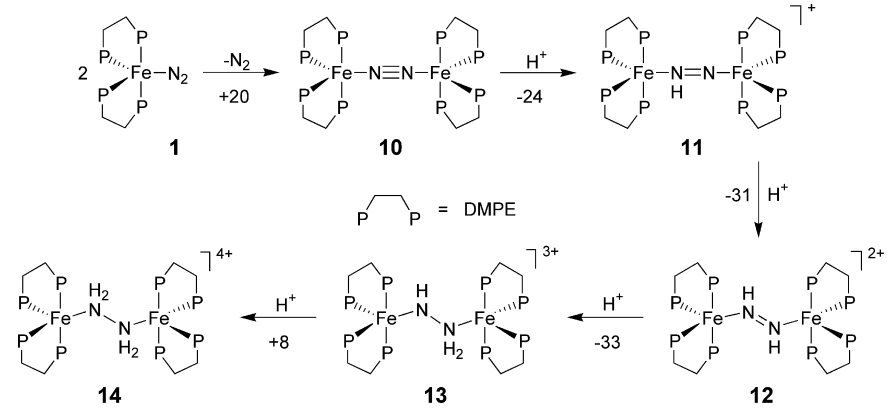

[a] Reaction energies are in kcal/mol.

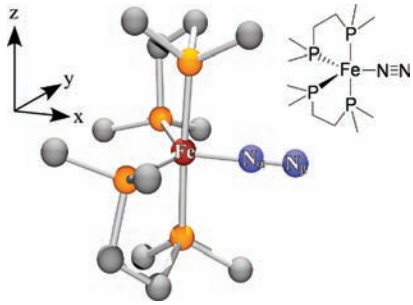

Figure 1. Optimized structure of $Fe(dmpe)_2N_2$ (**1**). Hydrogen atoms have been omitted for clarity. The axes chosen for describing the electronic structure are also shown.

Dinitrogen Complexes. $Fe(dmpe)_2N_2$ (1). The ground state of **1** is a singlet. The optimized singlet structure is trigonal bipyramidal (C_2 symmetry) with N_2 in an equatorial position (Figure 1), and the bond lengths and bond angles are in excellent agreement with those in the crystal structure of the closely related $Fe(depe)_2N_2$ complex[29] (Table 1). The Fe−N−N linkage is linear, and end-on binding of N_2 is preferred over side-on binding by 11 kcal/mol. The N−N bond length is slightly elongated (by 0.035 Å) upon binding to the metal center, compared to free N_2. The ν_{N-N} is significantly reduced upon binding (Table 2), and according to the Mulliken bond order analysis, most of the N−N triple-bond character is lost. Dissociation of N_2 from $Fe(dmpe)_2$ (**15**) costs 23 kcal/mol when calculated in vacuo. The $Fe(dmpe)_2N_2$ complex is stabilized in a THF solvent field by an additional 3 kcal/mol.

A molecular orbital diagram of complex **1** is given in Figure 2. Three orbitals are involved in Fe−N_2 binding. The highest occupied molecular orbital (HOMO; labeled d_{xy}_π_y*) can be described as an Fe d_{xy} orbital that is involved in the bonding of the equatorial phosphine ligands, as well as in bonding the dinitrogen via the π_y* orbital. The $d_{x^2-y^2}$ orbital is mostly nonbonding but also forms a bonding combination with the N_2 σ_g orbital. (The σ_g orbital is the orbital formed by overlap of the two sp hybridized orbitals on each N atom.) The Fe d_{xz} orbital mixes with the π_z* orbital (the d_{xz}_π_z* orbital). The Fe d_{z^2} and d_{yz} orbitals are nonbonding with respect to the dinitrogen ligand, but one admixture of these orbitals is involved in bonding the phosphine ligands.

Mulliken population analysis (MPA) indicates that significant negative charge (−0.31*e*) is transferred to the N_2 upon binding (Table 4). Much of this charge is transferred via π back-donation from the Fe d_{xy} and d_{xz} orbitals to the dinitrogen π_y* and π_z* orbitals, respectively. Most of the negative charge is transferred to the terminal nitrogen atom, N_β, suggesting that N_β is more susceptible to protonation than N_α.

$[FeH(dmpe)_2N_2]^+$ (2b). This complex is not an intermediate for any of the mechanisms examined, but it is the thermodynamic product of the protonation of complex **1**. Indeed, protonation at the metal center is calculated to be favorable by 58 kcal/mol, about 40 kcal/mol more favorable than protonation at the terminal nitrogen (**2a**; Scheme 1). Complex **2b** has octahedral coordination about the Fe, with the hydride trans to the N_2, in good agreement with the crystal structure of Hills et al.[32] The N−N bond length is close to that of free N_2, which also agrees well with the published structure. In the protonation reaction to form complex **2b**, the proton bonds to the Fe $d_{x^2-y^2}$ orbital, substantially lowering the energy of this orbital. There are two Fe−N π-bonding orbitals, which are mixtures of the Fe d_{xy} and d_{xz} orbitals and the dinitrogen π_y* and π_z* orbitals. Negative charge is transferred back to the iron−phosphine unit, making dinitrogen less activated for further protonation. Indeed, this complex is not a viable species in N_2 reduction, as the subsequent protonation of N_2 in this complex is highly unfavorable (33 kcal/mol), which agrees with experimental results obtained by Henderson in which further reaction of this complex to yield ammonia was not observed.[33] Despite the fact that the dinitrogen is poorly activated, the calculations predict an Fe−N_2 dissociation energy of about 23 kcal/mol in THF, only 3 kcal/mol less than for complex **1**. The lowest-energy triplet state is calculated to be about 30 kcal/mol higher in energy than that of the singlet.

The Asymmetric Monomer Mechanism. The asymmetric monomer mechanism and reaction energies are shown in Scheme 2. In this mechanism, the complex undergoes two successive protonations to the terminal nitrogen (N_β) fol-

(33) Henderson, R. A. *J. Chem. Soc., Dalton Trans.* **1988**, 515–520.

Table 1. Bond Lengths (Å) and Angles (deg) of Fe(dmpe)$_2$N$_2$ Intermediates Determined by Geometry Optimizations Using B3LYP/6-31G*

	Fe−P	Fe−N(α,β)	N−N	Fe−N−N	N−N−H
free N_2			1.105		
trans-N_2H_2			1.246		106.1
N_2H_4			1.437		111.8
(**1**) $[Fe-N_2]^0$	2.194−2.238	1.777	1.138	179.7	
exp.[29] $[Fe-N_2]^0$ (depe)	2.176−2.41	1.748	1.139		
(**2a**) $[Fe-N_2H]^+$	2.252−2.296	1.681	1.221	167.1	111.7
(**2b**) $[FeH-N_2]^+$	2.278−2.280	1.824	1.123	180.0	
exp.[32] $[FeH-N_2]^+$	2.1763−2.220	1.802−1.826	1.112−1.178	179.5−179.4	
(**3**) $[Fe-NNH_2]^{2+}$	2.309−2.338	1.663	1.265	179.9	121.2
(**4**) $[Fe-NNH_2]^0$	2.170−2.324	1.773	1.343	131.1	120.1−124.3
(**5**) $[Fe-N]^+$	2.246−2.299	1.529			
(**6a**) *trans*-$[Fe-NHNH]^{2+}$	2.273−2.373	1.890	1.257	131.1	109.3
(**6b**) *cis*-$[Fe-NHNH]^{2+}$	2.258−2.372	1.876	1.254	114.1	112.9−116.9
(**7**) $[Fe-NHNH]^0$	2.203−2.262	1.983	1.401	69.3	106.0
exp.[30] $[Fe-N_2H_2]^0$	2.162−2.202	2.016, 2.032	1.427	68.8−69.9	103.4−115.6
(**8**) $[Fe-NHNH_2]^+$	2.261−2.325	1.966, 1.983	1.437	69.3	106.3−115.3
(**9**) $[Fe-N_2H_4]^{2+}$	2.310−2.356	2.035, 2.037	1.451	69.0	110.8−111.0
exp.[30] $[Fe-N_2H_4]^{2+}$	2.196−2.260	1.981, 2.003	1.444	69.5	107.7−110.4
(**10**) $[Fe-N_2-Fe]^0$	2.191−2.245	1.856	1.153		
(**11**) $[Fe-N_2H-Fe]^+$	2.235−2.346	1.760, 1.887	1.289		
(**12**) $[Fe-N_2H_2-Fe]^{2+}$	2.296−2.344	1.852	1.420		
(**13**) $[Fe-N_2H_3-Fe]^{3+}$	2.275−2.408	1.889, 2.096	1.495		
(**14**) $[Fe-N_2H_4-Fe]^{4+}$	2.275−2.421	2.154, 2.434	1.491		

Table 2. Vibrational Frequencies (cm^{-1}) of Fe(dmpe)$_2$N$_2$ Intermediates Determined by Geometry Optimizations Using B3LYP/6-31G*

	ν_{N-N}	ν_{Fe-N}
free N_2	2458	
exp. N_2	2331	
free *trans*-N_2H_2	1664	
free N_2H_4	948	
(**1**) $[Fe-N_2]^0$	2133	521
exp.[5] $[Fe-N_2]^0$	1975	
(**2a**) $[Fe-N_2H]^+$	1738	602
(**2b**) $[FeH-N_2]^+$	2253	471
exp.[5] $[FeH-N_2]^+$	2094	
(**3**) $[Fe-NNH_2]^{2+}$	1515	598
(**4**) $[Fe-NNH_2]^0$	1134	643
(**5**) $[Fe-N]^+$		1104
(**6a**) *trans*-$[Fe-NHNH]^{2+}$	1557	527
(**6b**) *cis*-$[Fe-NHNH]^{2+}$	1597	528
(**7**) $[Fe-NHNH]^0$	1062	501, 544
(**8**) $[Fe-NHNH_2]^+$	960	479, 530
(**9**) $[Fe-N_2H_4]^{2+}$	1004	390, 419

Table 3. Mulliken Bond Order Analysis of Fe(dmpe)$_2$N$_2$ Intermediates

	Fe−P	Fe−N (Fe−N_β)	N−N	N−H
N_2			2.79	
N_2H^+			2.67	0.81
trans-N_2H_2			1.89	0.92
cis-N_2H_2			1.88	0.92
iso-N_2H_2			1.88	0.85
$N_2H_3^+$			1.93	0.82−0.91
N_2H_4			0.96	0.94−0.95
(**1**) $[Fe-N_2]^0$	0.47	0.86	2.27	
(**2a**) $[Fe-N_2H]^+$	0.40−0.45	1.27	1.67	0.88
(**2b**) $[FeH-N_2]^+$	0.38−0.39	0.57	2.48	
(**3**) $[Fe-NNH_2]^{2+}$	0.39−0.52	1.38	1.40	0.87
(**4**) $[Fe-NNH_2]^0$	0.34−0.52	1.43	1.09	0.90−0.92
(**5**) $[Fe-N]^+$	0.20−0.53	2.62		
(**6a**) *trans*-$[Fe-NHNH]^{2+}$	0.38−0.48	0.48	1.74	0.89−0.92
(**6b**) *cis*-$[Fe-NHNH]^{2+}$	0.41−0.50	0.45	1.73	0.87−0.89
(**7**) $[Fe-NHNH]^0$	0.59−0.63	0.77	1.00	0.95
(**8**) $[Fe-NHNH_2]^+$	0.57−0.67	0.35−0.65	0.93	0.91−0.94
(**9**) $[Fe-N_2H_4]^{2+}$	0.34−0.47	0.24−0.25	0.92	0.90
(**10**) $[Fe-N_2-Fe]^0$	0.42−0.44	0.62, 0.62	2.00	
(**11**) $[Fe-N_2H-Fe]^+$	0.31−0.48	1.16, 0.74	1.33	0.84
(**12**) $[Fe-N_2H_2-Fe]^{2+}$	0.34−0.46	0.94, 0.94	0.99	0.91
				0.91
(**13**) $[Fe-N_2H_3-Fe]^{3+}$	0.31−0.56	0.88, 0.28	0.92	0.92
				0.91, 0.91
(**14**) $[Fe-N_2H_4-Fe]^{4+}$	0.34−0.59	0.20, 0.21	0.95	0.88−0.90

lowed by a two-electron reduction by complex **1**. Subsequent protonation of N_β in complex **4** results in the formation of NH_3.

$[Fe(dmpe)_2NNH]^+$ (2a). Formation of this complex via protonation of the terminal nitrogen of **1** is favorable by 18 kcal/mol. The five-coordinate complex displays trigonal bipyramidal geometry. The N−N bond is elongated upon protonation, and the Fe−N−N angle is slightly distorted from linear. End-on binding is preferred over side-on binding by about 8 kcal/mol. Protonation results in further weakening of the N−N bond, as shown by the reduced N−N stretching frequency and further reduction in the N−N bond order. Protonation also results in strengthening of the Fe−N bond, as shown by the 0.1 Å decrease in the Fe−N bond length and substantial increase in bond order. The terminal nitrogen, N_β, has a trigonal planar geometry, suggesting some sp^2 character. The protonated N_2 is bound very tightly to the complex, having a dissociation energy of 109 kcal/mol. The complex becomes more polarized, in the sense that more positive charge is transferred to the iron and more negative charge (−0.5*e*) to the dinitrogen, with the terminal nitrogen slightly retaining the majority of that negative charge. The greater negative charge on the terminal nitrogen suggests that N_β is more primed than the coordinating nitrogen for the addition of a second proton. The bonding of the newly added proton involves the d_{xy}–π_y* orbital and the dinitrogen π_y orbital, effectively eliminating the triple bond. The lowest-energy triplet state is calculated to be about 2 kcal/mol lower in energy than the singlet. The calculations indicate that the triplet state is stabilized by the solvent field by 14 kcal/mol over the singlet, which may be due to the larger dipole moment for the triplet (4.6 D) compared to the singlet (3.9 D). Calculations were also performed on an isomer in which the proton was added to the proximal nitrogen, N_α, of complex **1**. However, all attempts to optimize this structure resulted in metal hydride formation (**2b**) vide supra.

$[Fe(dmpe)_2NNH_2]^{2+}$ (3). Further protonation of **2a** at the terminal nitrogen results in the formation of the *iso*-diazene

Table 4. Atomic charges of $Fe(dmpe)_2N_2$ Intermediates from Mulliken Population Analysis

	Fe	P	N_α	N_β	H
trans-N_2H_2			−0.23	−0.23	0.23
N_2H_4			−0.45	−0.45	0.22
NH_3			−0.67		0.22
(**1**) $[Fe-N_2]^0$	0.04	0.47−0.54	−0.09	−0.22	
(**2a**) $[Fe-N_2H]^+$	0.27	0.53−0.54	−0.22	−0.28	0.24
(**2b**) $[FeH-N_2]^+$	−0.05	0.58−0.59	−0.03	−0.09	−0.05[a]
(**3**) $[Fe-NNH_2]^{2+}$	0.31	0.54−0.59	−0.25	−0.20	0.31
(**4**) $[Fe-NNH_2]^0$	−0.08	0.50−0.55	−0.41	−0.35	0.20−0.22
(**5**) $[Fe-N]^+$	0.15	0.51−0.57	−0.33		
(**6a**) *trans*-$[Fe-NHNH]^{2+}$	0.65	0.49−0.54	−0.27	−0.19	0.25−0.30
(**6b**) *cis*-$[Fe-NHNH]^{2+}$	0.53	0.52−0.55	−0.28	−0.16	0.26−0.30
(**7**) $[Fe-NHNH]^0$	0.29	0.49−0.53	−0.47	−0.47	0.20
(**8**) $[Fe-NHNH_2]^+$	0.52	0.48−0.52	−0.50	−0.43	0.21−0.27
(**9**) $[Fe-N_2H_4]^{2+}$	0.67	0.46−0.54	−0.44	−0.44	0.29−0.31
(**10**) $[Fe-N_2-Fe]^0$	0.27, 0.27	0.46−0.48	−0.20	−0.20	
(**11**) $[Fe-N_2H-Fe]^+$	0.40, 0.30[b]	0.44−0.56	−0.38	−0.38	0.33
(**12**) $[Fe-N_2H_2-Fe]^{2+}$	0.40, 0.42	0.48−0.56	−0.49	−0.49	0.25, 0.27
(**13**) $[Fe-N_2H_3-Fe]^{3+}$	0.45, 0.68[b]	0.44−0.60	−0.58	−0.43	0.26−0.29
(**14**) $[Fe-N_2H_4-Fe]^{4+}$	0.56, 0.67	0.46−0.59	−0.44	−0.44	0.28−0.30

[a] This H corresponds to the iron-bound hydride. [b] This value corresponds to the iron bound to the more protonated nitrogen atom.

complex, **3**. This protonation is exothermic by 6 kcal/mol, and exergonic by 3 kcal/mol. The triplet form of this structure is calculated to be only 3 kcal/mol higher in energy. There is an additional increase in the N−N bond length and a corresponding decrease in the Fe−N bond length. The Fe−N−N angle is linear. The N−N stretch is computed to be 1515 cm^{-1}. The Fe−N and N−N bond orders are nearly equal at about 1.4, suggesting that both bonds have significant double-bond character. The *iso*-diazene molecule is bound to the $[Fe(dmpe)]^{2+}$ unit with a dissociation energy of 32 kcal/mol. Despite the addition of another positive charge via protonation, there is still substantial negative charge present on the nitrogen atoms, although the MPA assigns slightly more negative charge to N_α. The net charge of the diazene is slightly positive (0.17*e*), suggesting a formal oxidation state of +2 for iron in this complex. Binding of the Fe to the dinitrogen involves primarily the d_{xy}–π_y* and d_{xz}–π_z* orbitals. Protonation of N_β or N_α to form $[Fe(dmpe)_2N_2H_3]^{3+}$ is very unfavorable (by 41 and 24 kcal/mol, respectively). The two-electron reduction of **3** by **1** to form the *iso*-hydrazido complex **4** is less endothermic than either protonation. Thus, this pathway to form the *iso*-hydrazido complex (**4**) is considered as the next step.

$Fe(dmpe)_2NNH_2$ (4). The two-electron reduction of **3** is endothermic by 18 kcal/mol, but endergonic by only 1 kcal/mol. This is due to the large increase in entropy resulting from the dissociation of N_2 from the oxidized $Fe(dmpe)^{2+}$ complex **16**. The Fe−N−N angle of complex **4** is about 131°, suggesting an sp^2-hybridized N_α. The Fe−N bond increases by over 0.10 Å in length, but the Fe−N bond order indicates slightly more double-bond character. The N−N bond loses most of its double-bond character, elongates by 0.08 Å, and is intermediate between that calculated for free *trans*-diazene and that calculated for hydrazine. The N−N−H angles are in the range suggesting an sp^2 N_β. Both nitrogen atoms carry significant negative charge and are ready for further protonation.

$[Fe(dmpe)_2N]^+$ (5). Protonation of complex **4** at N_β forms an unstable $[Fe(dmpe)_2NNH_3]^+$ complex, which leads to the spontaneous dissociation of ammonia. This process is calculated to be extremely exothermic (−53 kcal/mol) and exergonic (−65 kcal/mol). The remaining Fe−N bond shows mostly triple-bond character. Protonation of this complex is favorable (−8 kcal/mol), but the addition of two more protons to form $[Fe(dmpe)_2NH_3]^{4+}$ becomes highly unfavorable (over 60 kcal/mol). Therefore, another two-electron reduction by **1** would likely be required before a second equivalent of ammonia could be released.

Symmetric Monomer Mechanism. The symmetric monomer mechanism and reaction energies are shown in Scheme 3. This mechanism involves protonation steps which alternate between the two nitrogen atoms. Electron transfer occurs after the second protonation step and is followed by two additional protonations, resulting in an η^2-hydrazine complex.

$[Fe(dmpe)_2$(*trans*-NHNH)$]^{2+}$ (6a) and $[Fe(dmpe)_2$(*cis*-NHNH)$]^{2+}$ (6b). Symmetric protonation of **2a** to yield either *trans*- or *cis*-diazene structures is nearly thermoneutral (−2 to 0 kcal/mol, −1 to +1 with thermal and entropic corrections), with the trans form (**6a**) being about 2 kcal/mol more stable the cis form (**6b**). This is very close to the calculated energy difference (2.6 kcal/mol) between the free forms of *trans*- and *cis*-diazene. The triplet forms of **6a** and **6b** are calculated to be about 3 kcal/mol more stable than their corresponding singlet forms. Both **6a** and **6b** exhibit a square-pyramidal structure about the iron, which implies that the iron may take on octahedral coordination in this state. Yet, the calculations showed only a bent, end-on coordination for the diazene, with an Fe−N−N angle of 131° for the trans and 114° for the cis forms. (Optimizations of side-on configurations were attempted, but most of them resulted in structures in which the dinitrogen bonded end-on to the iron, except when symmetry was enforced.) The N−N bond lengths are very similar to each other and to the *iso*-diazene form (**3**); they are roughly 0.01 Å more elongated than the free form of *trans*-diazene obtained from DFT optimizations. The N−N bond orders of the trans and cis forms indicate more double-bonded character than for the iso form, but they are slightly less than that of free *trans*-diazene. However, the Fe−N bonds of the trans and cis forms are over 0.2 Å longer than those of the iso form, and the Fe−N bond order of about 0.5 suggests that the diazene is only weakly bound to the iron−phosphine complex. Indeed, the dissociation energy of the diazene from the complex in either form is only about 15 kcal/mol. The charge distributions of the trans and cis forms are also similar to that of the iso form except that there is more positive charge on the iron in **6a** and **6b**, suggesting more ionic character in the bonding between the complex and the diazene. This is consistent with the calculated binding energies being significantly weaker for these ligands with the complex. The bonding between the iron and diazene involves a σ bond between the Fe $d_{x^2-y^2}$ orbital and diazene sp^2-like orbital. Subsequent protonation of N_β in **6a** is endothermic by 20 kcal/mol. If the protonated species is formed, the release of $N_2H_3^+$ from $[Fe(dmpe)_2]^{2+}$ (**16**) is calculated to be slightly endothermic (4 kcal/mol) but exergonic by 10 kcal/mol. However, the outer-sphere

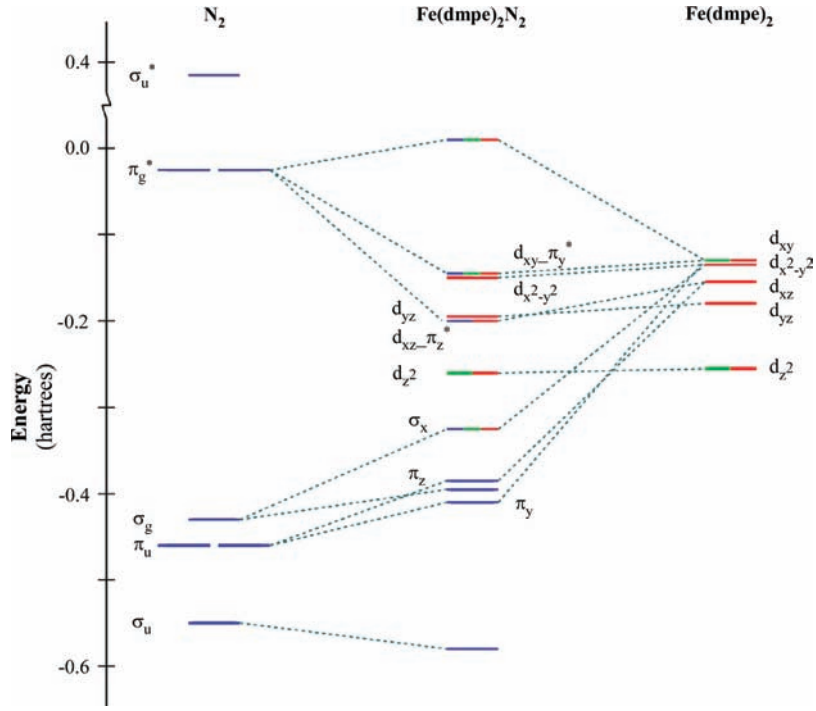

Figure 2. Energy level scheme for the bonding between N_2 and Fe(dmpe)$_2$ (**15**). The blue color indicates contributions from dinitrogen, red from iron, and green from phosphine. Other contributions are ignored, for clarity.

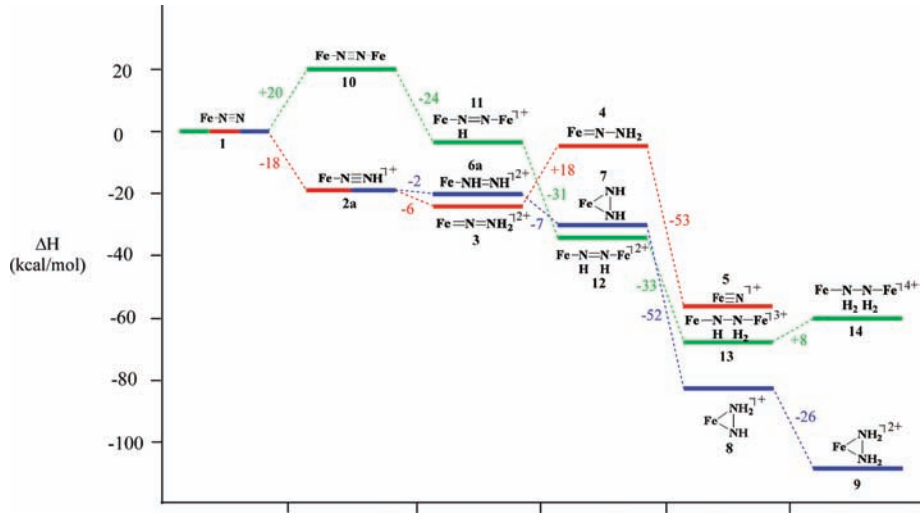

Figure 3. Calculated energy profile for the three schemes: asymmetric monomer mechanism (red), symmetric monomer mechanism (blue), and symmetric dimer mechanism (green). These energies do not include thermal and entropic corrections.

two-electron reduction of complex **6a** by **1** resulting in **7** is calculated to be exothermic by about 7 kcal/mol and exergonic by 21 kcal/mol and will be considered in more detail.

***cis*-Fe(dmpe)$_2$NHNH (7).** The *trans*-diazene binds side-on to the iron in this oxidation state, yielding pseudo-octahedral coordination about the iron. Side-on binding is preferred over the end-on binding form (**4**) by about 25 kcal/mol. This is in good agreement with a recent crystal structure of the Fe(dmpe)$_2$(N_2H_2) complex, which shows that the diazene is bound side-on to the iron.[30] The Fe−P bonds are overestimated by about 0.04−0.06 Å compared to the crystal structure values, and the Fe−N and N−N bonds are underestimated by 0.05 and 0.03 Å, respectively. Overall, the nature of the Fe−N and N−N bonding is well described by DFT. Field et al. describe this as an Fe^0−diazene complex. However, on the basis of the evidence presented below, the complex is perhaps better described as an Fe^{II}−hydrazido(2−) complex. The length of the N−N bond is over 0.15 Å longer than that computed for free *trans*-diazene and is much closer to that of free hydrazine. In addition, when **6a** is reduced to form **7**, the N−N bond length increases by about 0.14 Å and the bond order decreases to 1.0. Thus, all double-bonded character is lost. There is also a substantial decrease in ν_{N-N} (from 1557 to 1062 cm^{-1}). The Fe−N bond length increases by about 0.09 Å over complex **6a**, while the Fe−N bond order also increases. The dissociation energy of *trans*-diazene from $[Fe(dmpe)_2]^0$ is computed to be about 47 kcal/mol. The HOMO is mostly antibonding between the iron and diazene, with some overlap between the Fe $d_{x^2-y^2}$

orbital and the diazene sp^2-like π_z^* orbital. The greatest contributions to the Fe−hydrazido bonding come from σ bonds formed by the Fe 4s and d_{z^2} orbitals with the dinitrogen π_x orbital, and π bonds between Fe $d_{xz/xy}$ and π_x^*, and between Fe d_{yz} and π_z^*. The back-donations from the Fe substantially increase the charge distribution on each nitrogen, resulting in a net negative charge (−0.54*e*) on the hydrazido, making it a likely site for further protonation.

***cis*-[Fe(dmpe)$_2$NHNH$_2$]$^+$ (8).** This complex can be formed by the protonation of **7** at N_β (−52 kcal/mol). The protonated hydrazido(1−) molecule remains side-on bound to the iron center, maintaining octahedral coordination of the iron. There is a 0.036 Å increase in the N−N bond and a slight reduction in N−N bond order. Interestingly, there is substantial decrease in Fe−N bond order, yet a slight (0.017 Å) decrease in the Fe−N_α bond length. The Fe−N_β bond length is unchanged at 1.983 Å. These small structural changes upon protonation suggest a low energy barrier for this step. There is still a net negative charge on the hydrazido (over −0.20*e*), and the charge distribution suggests that the singly protonated N_α (−0.50*e*) would be more susceptible to additional protonation than the doubly protonated N_β (−0.43*e*).

***cis*-[Fe(dmpe)$_2$(N$_2$H$_4$)]$^{2+}$ (9).** Formation of this complex via protonation of **8** is also thermodynamically downhill (26 kcal/mol). The N−N bond length, bond order, and ν_{N-N} are mostly unchanged, but the Fe−N bond length increases to 2.036 Å and the Fe−N bond orders decrease to 0.25. The predicted side-on binding of hydrazine to the iron is in very good agreement with the reported structure of *cis*-[Fe(dmpe)$_2$(N$_2$H$_4$)]$^{2+}$.[30] The Fe−P and Fe−N bonds are overestimated (by 0.08 Å and 0.04 Å, respectively), but the N−N bond is very close (0.01 Å) to that reported in the crystal structure. The dissociation energy of N_2H_4 from complex **9** is calculated to be +24 kcal/mol in THF. The main Fe−N bonding MO is a strong π bond between the Fe d_{xy} and the dinitrogen π_x^* orbitals (the d_{xy}_π_x^* orbital). The HOMO is mostly antibonding between the iron and hydrazine, although there is some overlap between the nitrogen sp^3 hybrid orbitals and the Fe $d_{x^2-y^2}$ orbital. There is a net positive charge (∼0.30*e*) on the hydrazine. Further protonation of this complex results in the dissociation of $N_2H_5^+$ from [Fe(dmpe)$_2$(N$_2$H$_5$)]$^{3+}$, with the net process being slightly endothermic (6 kcal/mol) but exergonic (−8 kcal/mol). Protonation and subsequent dissociation of NH_3 from [Fe(dmpe)$_2$(N$_2$H$_5$)]$^{3+}$ was also considered and found to be endothermic by 48 kcal/mol.

Symmetric Dimer Mechanism. The intermediates and reaction energies for the symmetric dimer mechanism are shown in Scheme 4. The first step involves the formation of a dinitrogen-bridged dimer, followed by four successive protonation steps, resulting in the formation of a hydrazine intermediate.

Fe$_2$(dmpe)$_4$N$_2$ (10). The formation of this complex via dimerization of complex **1**, resulting in the liberation of N_2, is calculated to be unfavorable by 20 kcal/mol. The geometry optimization yielded a structure in which the second Fe(dmpe)$_2$ is rotated almost 90° with respect to the first Fe(dmpe)$_2$. Both Fe atoms bind to the dinitrogen in linear (180°) fashion. The N−N bond length in the dimer is slightly (0.015 Å) longer than in **1**, but the Fe−N bond lengths are nearly 0.08 Å longer. This is consistent with the bond order analysis, which indicates that the N−N and Fe−N bonds are weaker for the dimer than for **1**. In fact, formation of the dimer results in fully eliminating the triple-bond character of the N−N bond. The MPA indicates that both nitrogen atoms in **10** have the same charge as the terminal nitrogen (N_β) of **1**, and the dinitrogen overall has a more negative charge in the dimer than in **1**. The slight elongation of the N−N bond length over the monomer complex and the transfer of more negative charge to the N_2 suggest that formation of a dimer would further activate N_2 for reduction. Once formed, the complex itself has limited stability; the dissociation of complex **10** into Fe(dmpe)$_2$ and **1** is unfavorable by only 6 kcal/mol. The two HOMOs of **10** are interesting. They can be described as linear combinations of the d_{xy}_π_y and d_{xz}_π_z orbitals. The HOMOs are significantly higher in energy than those of the monomer complex, and the HOMO−LUMO gap is much smaller, suggesting that this complex should be much more reactive. Each Fe is able to participate in the d_{xy}_π_y^* and d_{xz}_π_z^* backbonding, and these modes are stabilized by the extra Fe atom with respect to complex **1**.

[Fe$_2$(dmpe)$_4$N$_2$H]$^+$ (11). Formation of this complex via protonation of **10** is favorable by 24 kcal/mol, about 6 kcal/mol more favorable than the protonation of **1** to yield **2a**. Formation of this complex from the dimerization of **1** and **2a** (resulting in the loss of N_2) was also considered but found to be unfavorable by 15 kcal/mol. The proton bonds to the d_{xy}_π_y^* orbital on N_β. The N−N bond is elongated by 0.07 Å, and the double-bonded character of the N−N bond is greatly reduced, having less double-bonded character than that of the monomer complex **2a**. Despite the fact that the two nitrogen atoms are not equivalent, both nitrogen atoms have nearly the same charge. Both nitrogen atoms are more negatively charged than those in **2a**, with the unprotonated N_α having twice the negative charge compared to the corresponding N_α in **2a** (Table 4). The increased negative charge and N−N bond length suggest that this complex is more activated than **2a**. If formed, **11** could dissociate into [Fe(dmpe)$_2$N$_2$H]$^{0+}$ and [Fe(dmpe)$_2$]$^+$ (−5 kcal/mol).

[Fe$_2$(dmpe)$_4$N$_2$H$_2$]$^{2+}$ (12). Formation of this complex via protonation of **11** is favorable by 31 kcal/mol. This dimer can also be formed by the dimerization of **1** and **6a**, which is favorable by 14 kcal/mol. The N−N bond length is similar to but slightly longer (by 0.02 Å) than that of the hydrazido complex **7**, but the Fe−N bond lengths are more representative of the monomer diazene complexes (**6a** and **6b**). The N−N bond has no double-bond character, in contrast to **6a** and **6b**, which both contain significant double-bond character. The charge distributions of the nitrogen atoms are similar to, but slightly greater than, that of the hydrazido complex **7**. If formed, **12** could dissociate into [Fe(dmpe)$_2$N$_2$H$_2$]$^+$ and [Fe(dmpe)$_2$]$^+$ (−16 kcal/mol).

[Fe$_2$(dmpe)$_4$N$_2$H$_3$]$^{3+}$ (13). Protonation of **12** is favorable by 33 kcal/mol. The N−N bond length is comparable to that

of free hydrazine and is longer than any of the intermediates in the symmetric monomer mechanism. More negative charge is transferred to the singly protonated nitrogen, similar to that of **8**. If formed, **13** would energetically prefer to dissociate into **8** and **16** (−15 kcal/mol), although dissociation into $[Fe(dmpe)_2N_2H_3]^{2+}$ and $[Fe(dmpe)_2]^{+}$ would also be possible (−8 kcal/mol).

$[Fe_2(dmpe)_4N_2H_4]^{4+}$ (14). Protonation of **13** is unfavorable (+8 kcal/mol). The N−N bond length shortens slightly. The structure becomes asymmetric, as there are two different Fe−N bond lengths (2.154 and 2.434 Å). The charge distribution also reflects this asymmetry. The asymmetry suggests that the complex is beginning to dissociate into complexes **9** and **16**. Indeed, the complete dissociation into **9** and **16** is computed to be favorable by 45 kcal/mol.

Discussion

Fe−N_2 Binding Modes. The results of the DFT calculations show that dinitrogen compounds with double- or triple-bond character (N_2, N_2H, and all isomers of N_2H_2) prefer to coordinate end-on (η^1) rather than side-on (η^2). In the case of N_2, N_2H, and *iso*-diazene, end-on bonding involves a σ bond between the Fe $d_{x^2-y^2}$ orbital and the sp_x orbital of N_α, as well as two π bonds between the Fe d_{xy} and d_{xz} orbitals and the dinitrogen π_y* and π_z* orbitals, respectively. Dimer formation (complexes **10** and **11**) provides additional π back-bonding. For the *trans*- and *cis*-diazene complexes (**6a** and **6b**), end-on bonding involves a σ bond between the Fe $d_{x^2-y^2}$ orbital and a filled diazene sp^2-like orbital (see Figure S7, Supporting Information). Dinitrogen compounds with mostly single-bond character (hydrazido, hydrazine) prefer to bind in a side-on geometry (η^2). In addition to π back-bonding, this mode may also include σ and π bonding with the dinitrogen π orbitals (e.g., complex **7**).

Initial Site of Protonation. The calculations show that the terminal nitrogen in **1** has significant negative charge, suggesting that this is the site of initial protonation. Indeed, the first protonation of the terminal nitrogen to form **2a** is significantly downhill, with an energy of −19 kcal/mol. However, formation of the iron−hydride complex (**2b**) is nearly 40 kcal/mol more favorable than that of **2a** (Scheme 1). Much of this energy difference appears to come from the stabilization of the $d_{x^2-y^2}$ orbital in **2b** upon binding the proton when compared to **2a**. There is also much less back-bonding from the iron to the dinitrogen antibonding orbitals in complex **2b** compared to **2a**, which lowers the energies of the dinitrogen π-bonding orbitals, as well as the Fe d_{xy} and d_{xz} orbitals, contributing further to the energy difference between **2a** and **2b**. It is suggested that N_β is the kinetic protonation site and the Fe center is the thermodynamic protonation site. The terminal nitrogen is more exposed than the iron, so there is a higher probability that the proton will attack the terminal nitrogen. In addition, the complex has a dipole with the negative end on the terminal nitrogen and the positive end on the iron. The proton would thus be more attracted to the terminal nitrogen and repelled by the iron, further increasing the probability of attacking the nitrogen. Therefore, if the concentration of acid is low, the formation of **2a** is more likely to occur, but there may be sufficient time for it to isomerize to **2b** before another proton could be added. On the other hand, a high acid concentration would increase the probability of forming **3** (or **6a** or **6b**) from **2a**. At this point, further protonation of the iron center or isomerization to an iron−hydride is very unfavorable. The fact that protonation of the iron center is so thermodynamically favorable likely contributes to the small observed yields of ammonia and hydrazine in these systems. Experimental work and transition state calculations are underway to explore the kinetic barriers for these two protonation sites.

Protonation of Phosphine Arm. The basicity of the phosphine ligand makes it another potential protonation site. To get an idea of whether or not this could be a side reaction, additional calculations were performed where the iron−phosphine bond was broken and the free phosphine protonated. This was done for complexes **1**, **2a**, and **3**. Results of the newly optimized complexes indicated that protonation of the phosphine arm with triflic acid was unfavorable by 9 kcal/mol for complex **1**, 21 kcal/mol for complex **2a**, and 27 kcal/mol for complex **3**. In comparison, the first and second protonation of free dmpe by triflic acid was calculated to be −14 and −1 kcal/mol, respectively. Compared to the energetics for protonating the Fe atom or dinitrogen ligand, the protonation of the phosphine arm is not likely to interfere with the reduction of N_2, although such protonation may happen after the release of the nitrogen ligand.

Asymmetric Protonation of Fe(dmpe)$_2$N$_2$. Studies by Yandulov and Schrock[34] showed that the catalytic reduction of dinitrogen by molybdenum triamidoamine complexes occurs via one-electron reductions and addition of protons to the terminal nitrogen, resulting in the formation of ammonia and a molybdenum nitride complex. This nitride complex is then further reduced and protonated to yield a second equivalent of ammonia. Several intermediates (diazenido, hydrazido, imido, and amino) for this mechanism have been crystallized.[34] For the iron−dinitrogen system, the addition of the first two protons to the same nitrogen is the most favorable pathway. This is particularly interesting because the calculations indicate that free *iso*-diazene is 17 kcal/mol less stable than free *trans*-diazene, suggesting a 21 kcal/mol net stabilization of *iso*-diazene by the iron−phosphine complex. (This number was obtained by recalling that complex **3** is 4 kcal/mol more stable than complex **6a**.) Most of this stabilization comes from the significant π back-bonding from the iron that is not present in the trans or cis isomers. The addition of a third proton to complex **3** followed by a loss of ammonia and formation of an iron−nitride complex is significantly uphill ($\Delta E = 41$, $\Delta G = 32$ kcal/mol). While the two-electron reduction of **3** by complex **1** to yield an *iso*-hydrazido(2−) complex is only slightly endergonic ($\Delta G = 1$ kcal/mol), the ΔE value of 18 suggests a substantial enthalpic barrier. It is concluded that the asymmetric protonation of the coordinated dinitrogen is an unlikely pathway on the route to ammonia in this system.

Symmetric Protonation of Fe(dmpe)$_2$N$_2$. The symmetric protonation mechanism involves formation of an iron−diazene complex followed by the outer-sphere reduction via a

sacrificial $Fe(dmpe)_2N_2$ complex (Scheme 3). While the *iso*-diazene structure **3** has the lowest energy of all diazene isomers considered, the *trans*-diazene isomer is only 4 kcal/mol higher in energy, making it reasonably accessible by the direct protonation of **2a** or isomerization of **3**. Whereas the two-electron reduction of **3** is endergonic, the reduction of **6a** to **7** is exergonic (−21 kcal/mol). Once **7** is formed, two successive protonations of **7** to form complex **9** are highly favorable ($\Delta E = -78$, $\Delta G = -71$ kcal/mol total). Further protonation of complex **9** to give $N_2H_5^+$ and $[Fe(dmpe)_2]^{2+}$ is slightly favorable ($\Delta E = +6$, $\Delta G = -8$ kcal/mol), but the protonation of **9** followed by the dissociation of NH_3 from $[Fe(dmpe)_2NH_2]^{3+}$ was found to be highly unfavorable (by nearly 50 kcal/mol). Thus, the mechanism of ammonia formation from this complex is not clear at this time. However, it was shown experimentally that the treatment of *cis*-$[Fe(DMeOPrPE)_2(N_2H_4)]^{2+}$ with 1 M TfOH produces a mixture of $N_2H_5^+$ (64%) and NH_4^+ (21%) via a disproportionation reaction.[31] Therefore, this pathway produces both hydrazine and ammonia and is energetically favorable (−100 kcal/mol overall).

Outer-Sphere Electron Transfer. A major concern of the outer-sphere electron transfer reactions described above is the amount of reductant (complex **1**) remaining after the initial protonation reactions. Because the initial protonation of complex **1** is about 20 kcal/mol downhill, by the time appreciable amounts of **3** or **6** begin to form, only a minute concentration of **1** would be expected to remain. Thus, it is perhaps unlikely that there would ever be enough of **1** available to drive the production of NH_3 toward the 12−18% yields observed by Leigh and Jimenez-Tenorio[5] and Gilbertson et al.[6] One possibility is that other complexes downstream from **1**, such as **2a** or **7**, may participate in either one- or two-electron reductions. Experimental and theoretical studies involving these intermediates as potential reductants are currently underway.

Dimer Mechanism. Dimer formation is another means by which electron transfer may occur. The dimer mechanism involves the initial dimerization of two $Fe(dmpe)_2N_2$ complexes followed by four successive protonations, leading to a bridged hydrazine species (Scheme 4). At first, this appears to be an attractive mechanism because the first three protonations of the bridged dinitrogen are exothermic (−88 kcal/mol overall). However, the calculations show that the initial dimer-forming step leading to the formation of complex **10** is unlikely to occur (+20 kcal/mol). This result is consistent with the spectroscopic characterization of $Fe(DMeOPrPE)_2N_2$, which did not show any evidence for a bridged dinitrogen species.[6] The initial dimerization is a critical step for this mechanism because the protonation of the monomer is sufficiently favorable to prevent the formation of complex **10**.

It is possible that dimer formation occurs at other steps during the progress of the reaction. According to the calculations, dimer formation between complex **1** and complex **6a** to give complex **12** is possible (−14 kcal/mol). Once the diazene-bridged iron(0)/iron(II) complex is formed, further protonation to give the hydrazine dimer **14** is downhill. Complex **14** is unstable and prefers to dissociate into an $Fe^{II}(dmpe)_2$ fragment and the *cis*-hydrazine complex **9**. In fact, complexes **11**−**14** all prefer to dissociate back to their monomeric constituents. The inclusion of entropic corrections would further encourage this. Thus, while dimer formation may be possible (e.g., complex **12**), and protonation of these dimers is favorable, it is unlikely that the dimeric/bridged structure itself would be maintained during the course of the reaction. Unfortunately, the formation of dimer **12** from **1** and **6a** suffers from the same problem as the outer-sphere electron transfer mechanism described above. That is, there would be minimal amounts of **1** available to dimerize with **6a**. Alternative mechanisms in which electron transfer is not required are described next.

Disproportionation Mechanisms. It is possible that no electron transfer is required and that the first two protonation steps to form diazene are sufficient. Free diazene readily disproportionates in solution to N_2 and N_2H_4 (eq 2), and N_2H_4 could further disproportionate into N_2, H_2, and NH_3 (eq 3).

$$2N_2H_2 \rightarrow N_2H_4 + N_2 \quad (2)$$

$$3N_2H_4 \rightarrow 4NH_3 + N_2 \quad (3)$$

The dissociation energies of diazene in complexes **3**, **6a**, and **6b** range between 15 kcal/mol (*trans*-diazene) and 35 kcal/mol (*iso*-diazene). These results suggest that the iron−phosphine complex would stabilize the diazene, rather than promote disproportionation. Nevertheless, two disproportionation pathways were considered. One possibility is that another molecule, such as a solvent (THF) or counterion (triflate), could displace the diazene molecule, releasing it into solution (eqs 4 and 5).

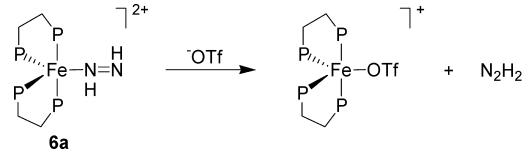

(4)

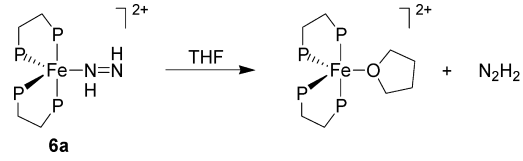

(5)

The binding of THF to the Fe^{II} form was found to be unfavorable, so THF is unlikely to displace diazene. However, the binding of triflate to the Fe^{II} form was found to be favorable by about 11 kcal/mol, which is comparable to the dissociation energy of *trans*-diazene. Because the difference in energy between the *trans*-diazene complex and the lower-energy *iso*-diazene complex is 4 kcal/mol, it is possible that, as *trans*-diazene is formed, it may be displaced by triflate. Because *trans*-diazene readily decomposes in solution, this would tend to drive the reaction toward the dissociation and disproportionation of diazene, leaving an iron−phosphine−triflate adduct. However, this mechanism leads to the

(34) Yandulov, D. V.; Schrock, R. R. *Inorg. Chem.* **2005**, *44*, 1103–1117.

Scheme 5. Mechanism Involving Iron Mediated Disproportionation of Diazene

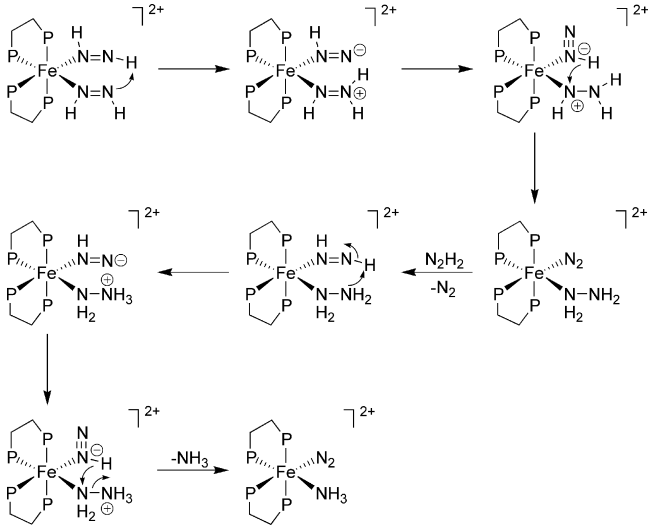

formation of N_2H_4 and does not account for the observed yields of NH_3.

Another disproportionation pathway involves a bis-diazene complex. Optimizations of **6a** and **6b** yielded a square-pyramidal structure, suggesting that the complex might accommodate another ligand to form an octahedral complex. It is possible that another diazene can bind at the vacant position, possibly involving dimer formation with another **6a** or **6b** complex. If two diazene molecules were to bind to the complex, the newly formed six-coordinate complex might facilitate the disproportionation of diazene into N_2 and N_2H_4 by keeping the two diazene ligands in close proximity (Scheme 5). The resulting N_2 could then be displaced by another diazene, with subsequent mediated disproportionation of the diazene and hydrazine to generate ammonia.

Conclusions

Density functional calculations were performed on several potential intermediates (but no transition states) for the reduction of N_2 to NH_3 by Fe(dmpe)$_2$. Three mechanisms were compared: an asymmetric monomer mechanism that involves successive protonation at the terminal nitrogen (Scheme 2), a symmetric monomer mechanism that proceeds through diazene and hydrazine intermediates (Scheme 3), and a dimer mechanism in which reduction takes place through a bridged dinitrogen species (Scheme 4).

The dimer mechanism involving a bridged dinitrogen has several exothermic protonation steps, but the calculations indicate that the critical step of forming a bridged dinitrogen intermediate is highly unfavorable. Formation of a bridging diazene intermediate is favorable, but it relies on the presence of a sacrificial Fe(dmpe)$_2$N$_2$, whose concentration may quickly vanish with an excess of strong acid. In addition, maintaining a dimer through each protonation step would be problematic, as each intermediate would prefer to dissociate into different monomeric intermediates.

Both monomer mechanisms begin with N_2 bonded in an end-on fashion to the Fe(dmpe)$_2$ moiety. Initial protonation at the terminal nitrogen forms **2a**, which is necessary in order to achieve NH_3 production and to avoid the formation of the inert thermodynamic product **2b**. The asymmetric addition of the second proton to form the *iso*-diazene complex **3** is slightly more favored than the symmetric addition to form **6a** or **6b**. However, additional protonation or two-electron reduction of this intermediate (complex **3**) is highly unfavorable.

The most favorable of the three mechanisms tested is the symmetric monomer mechanism. This pathway involves alternating protonation steps, first at the distal nitrogen followed by the proximal nitrogen to form **6a**. (Alternatively, the formation of **6a** could proceed through isomerization of **3**.) At this point, a two-electron reduction occurs by an outer-sphere mechanism from complex **1**, resulting in complex **7**. Successive protonations of **7** are sufficient to drive the production of $N_2H_5^+$, but the exact mechanism leading to ammonia formation remains unclear (although experimentally, we have shown disproportionation of N_2H_4 to NH_3 to be possible). Like the dimer mechanism, the symmetric monomer mechanism also relies on remaining amounts of Fe(dmpe)$_2$N$_2$, which in the presence of a strong acid may not be available in sufficient concentration at this point in the reaction. Should this be the case, the electron transfer step may involve other reductants such as **2a** or **7**.

Acknowledgment. We thank the Neuroinformatics Center at the University of Oregon for use of the ICONIC Grid, a high-performance computational infrastructure constructed with support from a National Science Foundation Major Research Instrumentation grant, NSF BCS-0321388. The NSF (NSF-CHE-0452004) is acknowledged for the experimental work in support of this study.

Supporting Information Available: Calculated structures for each mechanism; descriptions of the Fe(dmpe)$_2$ (**15**) and [Fe(dmpe)$_2$]$^{2+}$ (**16**) fragments; energy level diagrams for intermediates in Schemes 2−4; figures of bonding orbitals in complexes **1**, **3**, **6a**, **7**, **9**, and **10**; sample NWChem inputs; Cartesian coordinates for complexes **1**−**16**; total energies; and gross orbital populations. This material is available free of charge via the Internet at http://pubs.acs.org.

IC800930T